Direct Synthesis of Solvent-Free Multiwall Carbon Nanotubes/Silica Nonionic Nanofluid Hybrid Material

Jiao-Xia Zhang, Ya-Ping Zheng,* Lan Lan, Su Mo, Pei-Ying Yu, Wei Shi, and Ru-Min Wang

Department of Applied Chemistry, School of Natural and Applied Science, Northwestern Polytechnical University, Xi'an 710129, China

ABSTRACT The solvent-free nonionic nanofluid hybrid material consisting of multiwall carbon nanotubes (MWNTs) and silica nanoparticles is prepared by a facile route. The content of MWNTs/silica nanoparticles is up to 31 wt %. The hybrid material exhibits liquid-like behavior in the absence of solvent at 45 °C, which is a wax solid at room temperature. The process of melting and solidification is reversible over many cycles.

KEYWORDS: carbon nanotubes · silica nanoparticles · nonionic nanofluid · hybrid material · solvent-free

The exploitation of the physicochemical properties of nanoparticles has recently attracted increasing interest because of their technological applications such as in sensors and nanoelectronic devices.[1−4] Synthetic hybrid nanomaterials exhibit remarkable physicochemical properties that do not exist in the individual components.[5−7]

Carbon nanotubes (CNTs) have a unique combination of outstanding chemical, mechanical, and electrical properties,[8,9] which have been the focus of scientific research. However, it is known that the lack of solubility as well as the intrinsic physical and chemical inertness hinders their application fields. The solubility and the functionalization on the side walls are necessary for CNTs if they are applied in wide fields.[10]

In general, the conventional functionalized methods made nanoparticles behave solid-like in the absence of solvent and did not undergo a microscopic solid-to-liquid transition below 150 °C.

It had been reported that nanoparticles covered with functionalized ionic organic compound exhibited liquid-like behavior in the absence of solvent. The solvent-free nanofluid was synthesized by attaching an ionic corona of flexible chains onto an inorganic oxide core such as SiO_2, γ-Fe_2O_3, or TiO_2.[11,12] The functionalized MWNTs with liquid-like behavior were synthesized by attaching a canopy of epoxy-terminated silicone chains onto the nanotubes. The waxy solid contained 85% w/w MWNTs and exhibited fluid behavior at ambient conditions.[13] By attaching octadecyl amine groups of polyethylene glycol (PEG) onto the MWNTs, the amount of MWNTs was 40 wt % and melted reversibly at room temperature to yield a homogeneous viscous fluid.[14]

In this experiment, the MWNTs decorated with silica nanoparticles as the core were first fabricated *via* a facile chemical method, and the particular hybrid nanoparticle-capped nonionic modifier was engineered to a single homogeneous phase and exhibited liquid-like behavior at 45 °C.

RESULTS AND DISCUSSION

The solvent-free nonionic nanofluid hybrid material of MWNTs decorated with silica nanoparticles is shown in Scheme 1. It was prepared by a simple facile method. First, colloidal silica was dispersed in a 3-(trimethoxysilyl)-1-propanethiol (TSP) aqueous solution to enhance silica nanoparticle dispersion. As we know, nanoparticles intended to flocculate and agglomerate without modification. In order to restrain flocculation of silica nanoparticles, the 3-(trimethoxysilyl)-1-propanethiol was utilized to modify silica nanoparticles. Then the solvent-free hybrid nonionic nanofluids of MWNTs decorated with silica nanoparticles were fabricated by carboxylic MWNTs and PEO-*b*-PPO-*b*-PEO. The surface of carboxylic MWNTs created polar hydrophilic groups (−COOH, C═O, −OH) in order to enhance activity of the ends and side walls of MWNTs. Those groups were indispensable for MWNTs to further react with other groups. In our study, poly(ethylene

*Address correspondence to zhengyp@nwpu.edu.cn.

Received for review May 12, 2009 and accepted July 24, 2009.

Published online July 29, 2009.
10.1021/nn900557y CCC: $40.75

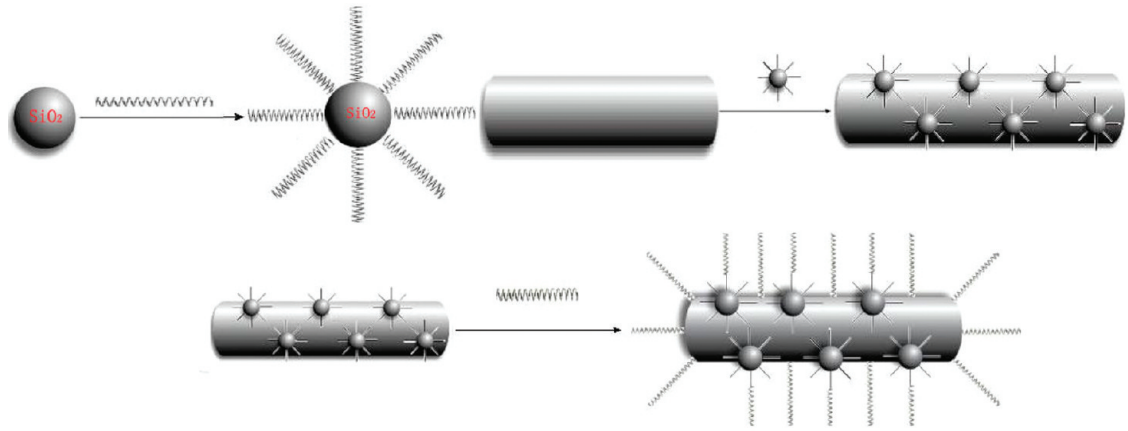

Scheme 1. Synthetic route of nonionic nanofluid hybrid material of MWNTs decorated with silica nanoparticles.

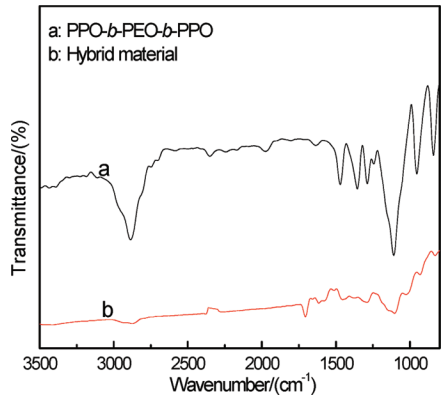

Figure 1. FTIR spectra of (a) PEO-*b*-PPO-*b*-PEO, (b) nonionic nanofluid hybrid material of MWNTs decorated with silica nanoparticles.

oxide)-*block*-poly(propylene oxide)-*block*-poly(ethylene oxide) (PEO-*b*-PPO-*b*-PEO) reacted with the −COOH, C═O, and −OH groups on the surface of carboxylic MWNTs *via* hydrogen bonding.

The groups on the hybrid material of MWNTs decorated with silica nanoparticles were studied by FTIR (Figure 1). Because TSP content in the hybrid material was very low, the curve of FTIR spectra lacked any TSP absorption bands. After reaction of the hybrid of MWNTs and silica nanoparticles with PEO-*b*-PPO-*b*-PEO, the FTIR spectra of the hybrid material showed the characteristic absorption peaks of PEO-*b*-PPO-*b*-PEO, such as C−O (1099 cm^{-1}), CH_3 (1450 cm^{-1}), and CH_2 (2847 and 2907 cm^{-1}).

The microstructure of MWNTs decorated with silica nanoparticles could be clearly observed from the TEM images (Figure 2). As shown in Figure 2a, the carboxylic MWNTs revealed the presence of typical hollow tubes. In the case of the hybrid material, well-distributed and isolated silica nanoparticles were found to densely ornament the walls of MWNTs uniformly. The TEM images revealed that the average diameter of spherical silica nanoparticles was <10 nm, and the TSP avoided further precipitation and aggregation of silica nanoparticles.

DSC was used to characterize the thermal properties of the hybrid material of MWNTs decorated with silica nanoparticles. The DSC heating trace of pure pluronic copolymer of PEO-*b*-PPO-*b*-PEO showed a large endothermic peak at 62 °C, which was the melting of

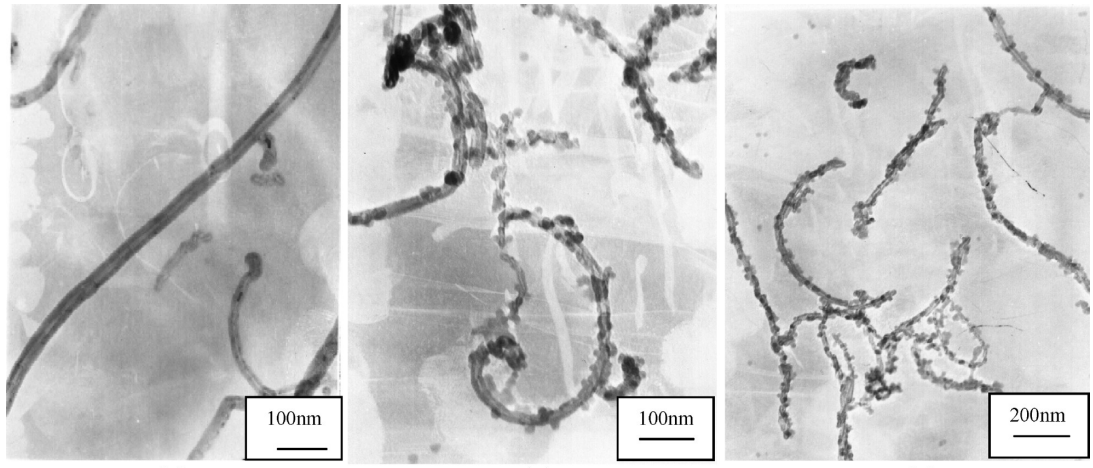

Figure 2. TEM images of (a) original MWNTs and (b) nonionic nanofluid hybrid material of MWNTs decorated with silica nanoparticles.

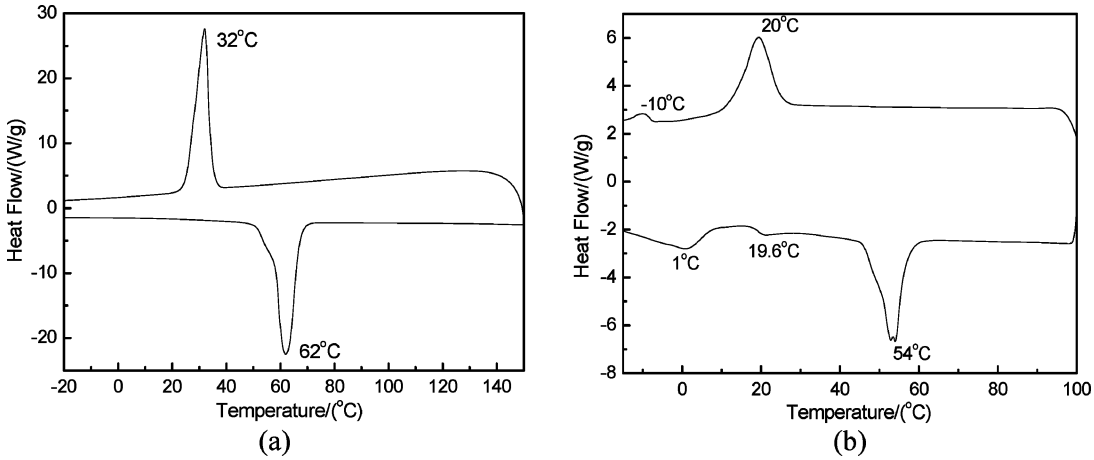

Figure 3. DSC curves of (a) PEO-*b*-PPO-*b*-PEO and (b,c) nonionic nanofluid hybrid material of MWNTs decorated with silica nanoparticles at different amplified times.

crystalline regions of PEO-*b*-PPO-*b*-PEO (Figure 3a), and the heat of fusion (ΔH_f) related to this phase transition was 124 J/g. The DSC cooling trace of pure PEO-*b*-PPO-*b*-PEO revealed a large exothermic peak at 32 °C, which corresponded to a crystallization of PEO-*b*-PPO-*b*-PEO, and the heat of crystallization (ΔH_c) related to this phase transition was 118 J/g. For the hybrid material, the DSC heating trace showed a second-order transition at 19.6 °C and an endothermic first-order transition at 54 °C, corresponding to the T_g and T_m of PEO-*b*-PPO-*b*-PEO, respectively (Figure 3b). The ΔH_f related to this phase transition was 37.5 J/g at 54 °C. The hybrid nanoparticles acted as nucleating agents for the PEO-*b*-PPO-*b*-PEO. In the meantime, they induced crystallization and increased the amorphous regions of the PEO-*b*-PPO-*b*-PEO. The increased amorphous regions explained the T_g appearance of hybrid material at 19.6 °C. The hybrid material, in the cooling process, exhibited an exothermic peak at 20 °C, corresponding to ΔH_c being 38.2 J/g. Because the hybrid nanoparticles acted as nucleating agents, it accelerated the sample fusion and crystallization at lower temperature. In addition, the melting peak at 1 °C and freezing peak at −10 °C may be caused by the residual water.

The content of the organic canopy on the surface of nanoparticles influenced the properties of hybrid material. So the TGA was carried out to confirm the thermal stability (see Figure 4). The TGA traces showed that the sample did not contain any residual solvent. The weight loss above 180 °C was due to decomposition of the organic alkyl groups. The organic and inorganic (MWNTs and silica nanoparticles) content was 69 and 31 wt %, respectively.

Usually, a dynamic spectrum can be used to understand the structures and properties of material. It is well-known that the dynamical storage modulus G′ and loss modulus G′′ of rheometrics mechanical spectrometry exhibit the relationship between the molecular motion and rheological behavior of the material.[15] Corresponding rheological behavior of the sample was carried out at 60 °C (Figure 5a). It showed that G′ and G′′ stay basically identical with the stress increasing. G′ embodies the elastic behavior of materials, which was the driving force of molecule deformation, and G′′ was the consumption energy of viscous deformation for materials.[16,17] It also showed that the G′′ for the hybrid material was higher than the G′. It suggested that the hybrid material was liquid material, whose G′′ was higher than the G′.[18] In addition, Figure 6 illustrates a complex fluid behavior of hybrid material at the full spectrum from the simple Newtonian fluid following the law of $G'(\omega) \propto \omega$ and $G''(\omega) \propto \omega$ at low angular frequency to non-Newtonian fluid at high angular frequency. The hybrid material was a waxy solid at room temperature, which undergoes solid-to-liquid transition at 45 °C, resulting in a fluid with considerably high viscosity (see Figure 5b). The process of melting and solidification was reversible over many cycles.

There are not enough theoretical bases to explain their fluidity. According to our supposition, the size and nature, such as the chain length, chain flexibility,

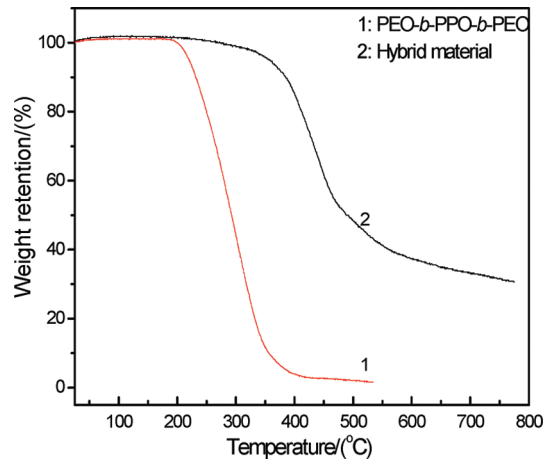

Figure 4. TGA traces of nonionic nanofluid hybrid material of MWNTs decorated with silica nanoparticles under nitrogen atmosphere.

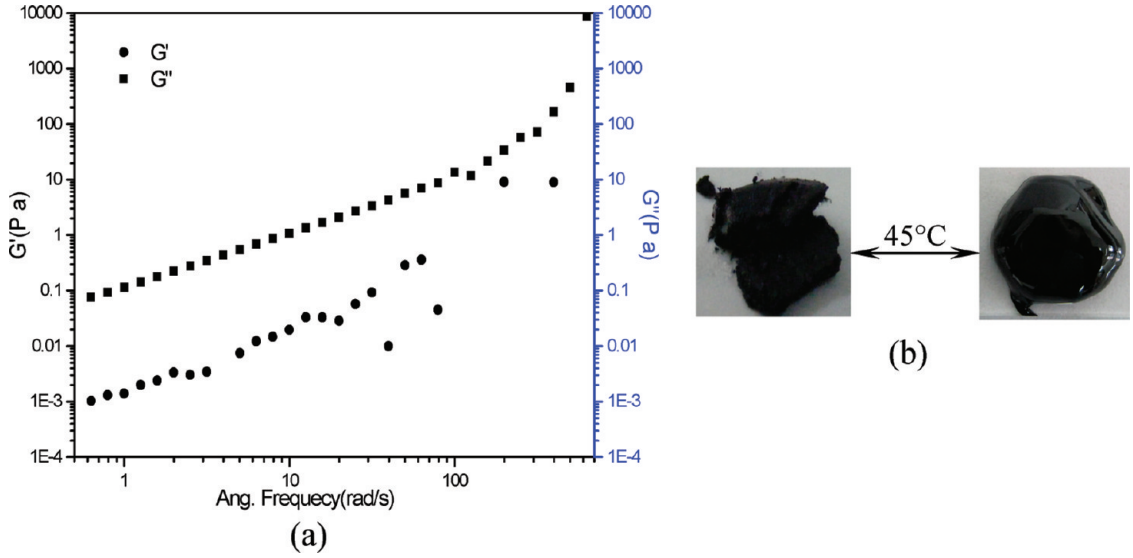

Figure 5. (a) Rheological behavior at 60 °C. (b) Reversible melting and solidifying behavior of nonionic nanofluid hybrid material.

and asymmetric structure of the modifier, are expected to significantly influence the building-up on the nanoparticle and interfacial and interparticle interaction and, further, the fluidity of the hybrid material. In addition, the grafting density on the core of the particles, the nature of the nanoparticle, and other factors also contribute to the fluid-like behavior. The 0.12 mg · g^{-1} hybrid material in deionized water was placed for a different time to observe their dispersion. Figure 6 showed that the concentration only decreased 4% from 0.12 to 0.115 mg · g^{-1} then trended to stability after placed for 200 h. Interaction between the modifier of the hybrid material and water prevents agglomeration and increases their dispersion and stability in water.

At last, the conductivity of the hybrid material in deionized water was investigated. As shown in Figure 8a, the electrical conductivity increased with the hybrid material volume fraction increasing. When the volume fraction was up to 15.2%, electrical conductivity increased slowly. This increase in conductivity suggested that an infinite network of percolated hybrid material started forming. The critical concentration of hybrid material, f_c, was calculated by the law $\sigma \propto (f - f_c)^t$,[19] where f is the volume fraction of filler. The conductivity exponent t generally reflects the dimensionality of the system with values typically around 1.3 and 2.0 for two and three dimensions, respectively. Figure 7a represents a percolation threshold of about 4.44 vol % and an exponent t of 0.34 for the hybrid material in water. The low value of $t = 0.34$ reflected the decrease in system dimensionality due to the MWNTs' high aspect ratio. Diffusion processes and particle−particle interaction forces played an important role in the agglomeration and network formation.[20] When the hybrid material volume fraction was less than f_c, the conductive network was not formation, so the conductivity was low. When the content increased up to f_c, the conductive network formed and the conductivity increased rapidly. Figure 7b shows the positive temperature coefficient for conductivity. The electron was easy to move with higher energy at higher temperature that led to the increase of conductivity. In addition, we found that the quality of the hybrid material dispersion had a pronounced effect on the conductivity in experiment.

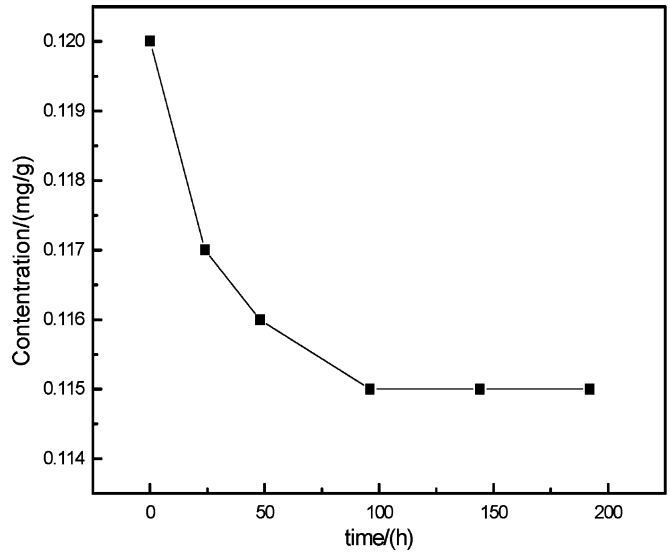

Figure 6. Curve of concentration *versus* time for hybrid material in water.

In summary, the capped hybrid nanomaterials consisting of MWNTs and silica nanoparticles were produced by a facile approach. The content of MWNTs and silica nanoparticles was up to 31 wt % in the capped hybrid material. The hybrid nanomaterial showed solid behavior at room temperature, which can flow at 45 °C. The process of melting and solidification was reversible over many cycles. It can be stable when dispersed

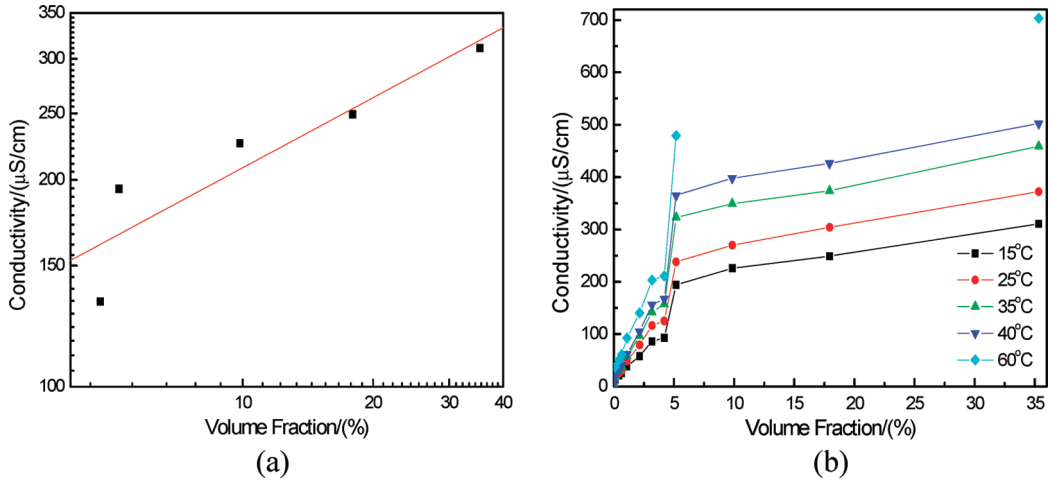

Figure 7. (a) Log−log plot of the conductivity *vs* volume fraction; (b) plot of the conductivity with volume fraction at different temperature.

in water for 200 h due to amphiphilic properties of the modifier molecule. The conductivity of the hybrid material exhibits that the percolation threshold is about 4.44 vol %.

EXPERIMENTAL SECTION

Materials and Preparation. The carboxylic MWNTs (>95%) were synthesized by chemical vapor deposition (CVD) and were provided by Chendu Organic Chemicals Co., Ltd. The diameter was about 20−30 nm, and the length was several micrometers. MWNTs were used in our experiment without further purification. 3-(Trimethoxysilyl)-1-propanethiol (TSP, 97%) was obtained from Momentive Performance Materials. The pluronic copolymer, PEO-*b*-PPO-*b*-PEO (M_n = 14 600, PEO = 82.5 wt %), and colloidal silica (HS30, surface area 220 m^2/g, concentration 30 wt %) were from Aldrich.

Colloidal silica was diluted with deionized water to a concentration of 10 wt %. To the suspension was added dropwise a dilute ethanol solution of TSP (8 wt %/wt) while stirring and then stirred at room temperature for 30 min; 0.1 g of carboxylic MWNTs was added into the silica/TSP solution and stirred for 30 min. At last, 100 mL of PEO-*b*-PPO-*b*-PEO (1 wt %) solution was added into the suspension and then stirred for 3 h, followed centrifugation at 8000 rpm for 30 min, resulting in a homogeneously black solution, and the supernatant liquid was collected, concentrated, and dried at 60 °C. The residual material was carefully rinsed with water and acetone several times to remove excess unreacted TSP and PEO-*b*-PPO-*b*-PEO. Finally, the product was dried at 60 °C until the weight was constant.

Characterization. The surface groups on the hybrid material were investigated by Fourier transform infrared (FTIR) spectrometry (WQF-310) using KBr pellets. Differential scanning calorimetry (DSC) traces were collected using a Q1000 TA Instruments at a heating rate of 10 °C/min. Thermogravimetric analysis (TGA) measurements were taken under N_2 flow by using TGAQ50 TA instruments. Transmission electron microscope (TEM) images were obtained at an accelerating voltage of 100 kV with the Joel H-600 instrument. For this study, a few drops of an aqueous dispersion of hybrid material were placed on a copper grid, and the solvent was evaporated prior to observation. Rheological properties were studied by using the rheometer of TA Instruments (AR-

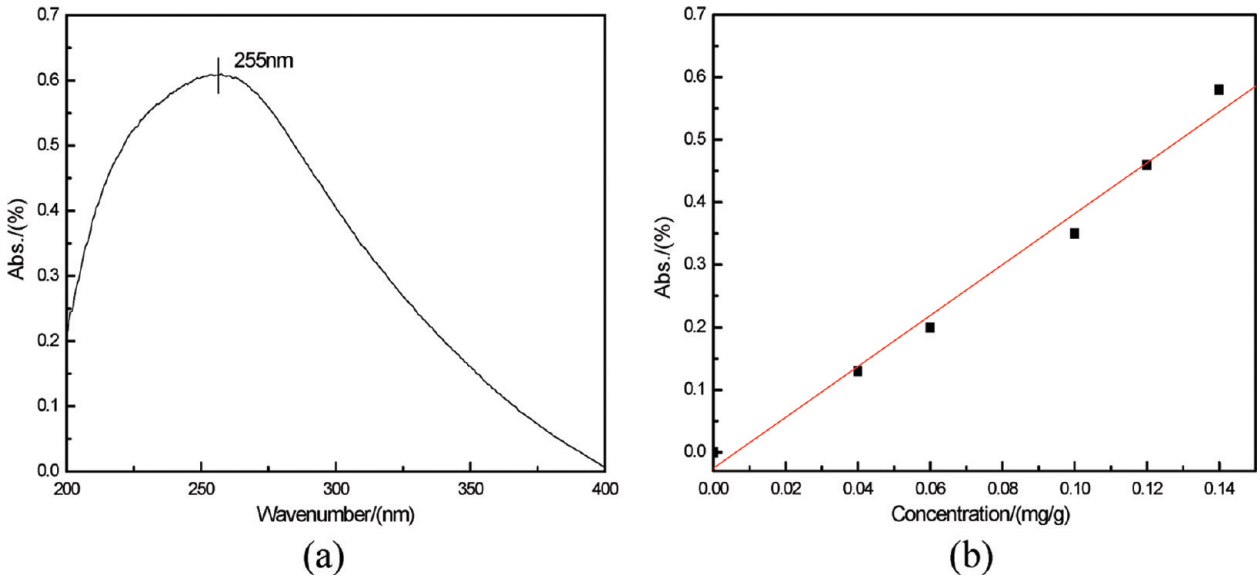

Figure 8. UV−vis adsorption spectrum of (a) linear calibration curve and (b) nonionic nanofluid hybrid material of MWNTs decorated with silica nanoparticles.

G2). The moduli G′ and G′′ were measured at a constant temperature in the stress range of 10−10 000 Pa. The controlled variable was 6.28 rad · s^{-1}. Then the conductivity apparatus was used to estimate the conductivity of the hybrid material. The dispersion of hybrid material in water was observed through an ultraviolet spectrophotometer (UV−vis). Water was a reference solution, and the samples with different concentration were scanned and then the linear calibration curve drawn (see Figure 8). We scanned the upper liquid after depositing a period time and then calculated their concentration to evaluate the dispersion of hybrid material.

Acknowledgment. We greatly acknowledge the fund supported by NPU Foundation for Fundamental Research (NPU-FFR-w018105), the Doctorate Foundation of Northwestern Polytechnical University (CX200816), and Shaanxi Natural Science Funds 2007(2007E108).

REFERENCES AND NOTES

1. Wohltjen, H.; Snow, A. W. Colloidal Metal−Insulator−Metal Ensemble Chemiresistor Sensor. *Anal. Chem.* **1998**, *70*, 2856–2859.
2. Zamborini, F. P.; Leopold, M. C.; Hicks, J. F.; Kulesza, P. J.; Malik, M. A.; Murray, R. W. Electron Hopping Conductivity and Vapor Sensing Properties of Flexible Network Polymer Films of Metal Nanoparticles. *J. Am. Chem. Soc.* **2002**, *124*, 8958–8964.
3. Tseng, R. J.; Huang, J.; Ouyang, J.; Kaner, R. B.; Yang, Y. Polyaniline Nanofiber/Gold Nanoparticle Nonvolatile Memory. *Nano Lett.* **2005**, *5*, 1077–1080.
4. Junno, T.; Carlsson, S. B.; Xu, H. Q.; Samuelson, L. Fabrication of Quantum Devices by Ångström-Level Manipulation of Nanoparticles with an Atomic Force Microscope. *Appl. Phys. Lett.* **1998**, *72*, 548–550.
5. Agrawal, S.; Kumar, A.; Frederick, M. J.; Ramanath, G. Hybrid Microstructures from Aligned Carbon Nanotubes and Silica Particles. *Small* **2005**, *1*, 823–826.
6. Guo, S. J.; Zhai, J. F.; Fang, Y. X.; Dong, S. J.; Wang, E. Nanoelectrocatalyst Based on High-Density Au/Pt Hybrid Nanoparticles Supported on a Silica Nanosphere. *Chem. Asian J.* **2008**, *3*, 1156–1162.
7. Mousavand, T.; Takami, S.; Umetsu, M.; Ohara, S.; Adschiri, T. Supercritical Hydrothermal Synthesis of Organic−Inorganic Hybrid Nanoparticles. *J. Mater. Sci.* **2006**, *41*, 1445–1448.
8. Coleman, J. N.; Khan, U.; Blau, W. J.; Gun'ko, Y. K. Small but Strong: A Review of the Mechanical Properties of Carbon Nanotube−Polymer Composites. *Carbon* **2006**, *44*, 1624–1652.
9. Baughman, R. H.; Zakhidov, A. A.; de Heer, W. A. Carbon Nanotubes—The Route toward Applications. *Science* **2002**, *297*, 787–792.
10. Chen, C. S.; Chen, X. H.; Xu, L. S.; Yang, Z.; Li, W. H. Modification of Multi-Walled Carbon Nanotubes with Fatty Acid and Their Tribological Properties as Lubricant Additive. *Carbon* **2005**, *43*, 1660–1666.
11. Bourlinos, A. B.; Herrera, R. A.; Chalkias, N.; Jiang, D. D.; Zhang, Q.; Archer, L. A.; Giannelis, E. P. Surface-Functionalized Nanoparticles with Liquid-like Behavior. *Adv. Mater.* **2005**, *17*, 234–237.
12. Bourlinos, A. B.; Chowdhury, S. R.; Herrera, R. A.; Jiang, D. D.; Zhang, Q.; Archer, L. A.; Giannelis, E. P. Functionalized Nanostructures with Liquid-like Behavior: Expanding the Gallery of Available Nanostructures. *Adv. Funct. Mater.* **2005**, *15*, 1285–1290.
13. Bourlinos, A. B.; Georgakilas, V.; Boukos, N.; Dallas, P.; Trapalis, C.; Giannelis, E. P. Silicone-Functionalized Carbon Nanotubes for the Production of New Carbon-Based Fluids. *Carbon* **2007**, *45*, 1583–1585.
14. Zhang, J. X.; Zheng, Y. P.; Yang, X. D.; Wang, R. M. The Synthesis of a Second Generation of Nanofluids Based on Carbon Nanotubes. *Acta Polym. Sin.* **2008**, 1209–1213.
15. Xu, P. X. *Polymer Rheology and Their Application*; Chemical Industry Press: Beijing, 2003; pp 3−13.
16. Yin, J. H.; Nie, J. Y.; Yang, J. S.; Hua, B. J. Study on the Cure Rheological Behavior of Epoxy Resin Composite. *Acta Mater. Compos. Sin.* **1992**, *9*, 103–109.
17. Guo, X. T.; Zhao, Y. M.; Ning, P.; Li, L. K. Dynamic Rheological Properties of PA6 Modified by Compound Amine. *China Plast. Ind.* **2006**, *34*, 35–38.
18. Wu, Q. H.; Wu, J. A. *Polymer Materials Rheology*. Higher Education Press: Beijing, 1994; pp 1−5.
19. Stauffer, D.; Aharnoy, A. *Introduction to The Percolation Theory*; Taylor and Francis: London, 1991; pp 73−86.
20. Sandler, J. K. W.; Kirk, J. E.; Kinloch, I. A.; Shaffer, M. S. P.; Windle, A. H. Ultra-Low Electrical Percolation Threshold in Carbon-Nanotube-Epoxy Composites. *Polymer* **2003**, *44*, 5893–5899.